




 Cite this: *RSC Adv.*, 2018, 8, 15587

 Received 18th January 2018
Accepted 20th April 2018

DOI: 10.1039/c8ra00526e

rsc.li/rsc-advances

Photoluminescence properties of a Ce³⁺ doped Sr₃MgSi₂O₈ phosphor with good thermal stability

 Baochen Wang,  Yangai Liu, * Zhaohui Huang  and Minghao Fang

This study mainly reports an investigation about the crystal structure and photoluminescence properties of a Ce³⁺ doped alkaline earth metal silicate Sr₃MgSi₂O₈. X-ray powder diffraction (XRD) and structure refinement methods are adopted to characterize the phase composition and crystal structure. The excitation/emission spectra and diffuse reflection spectra (DRS) of the title phosphor are measured and the mechanism of concentration quenching as well as thermal quenching are discussed in detail. Results show that the concentration quenching in Sr₃MgSi₂O₈ is due to dipole–dipole interaction energy transfer between Ce³⁺ ions. The title phosphor has an excellent thermal stability with 90% emission intensity reserve when the temperature rises to 150 °C. The related mechanism is considered to be the thermal ionization effect and an energy level diagram was proposed to show the thermal ionization process.

1. Introduction

In recent decades, white light emitting diodes (w-LEDs) have been replacing conventional incandescent and fluorescent lamps for general illumination due to their overwhelming merits such as long life, being energy saving, and their environmental friendliness as well as high efficiency.^{1–3} Although LEDs have been applied in many fields, the luminescence properties of w-LEDs for general illumination still need to be improved in terms of their color rendering index (CRI) and correlated color temperature (CCT).^{4,5} The first and most common w-LED, which is fabricated with a blue LED chip and yellow-emitting YAG:Ce³⁺ phosphor, suffers from many drawbacks such as poor CRI ($R_a = 70$ to 80) and high CCT (approximately 7750 K).^{3,6} To achieve “warmer” white light with high CRI, a strategy combining a blue-LED and yellow-emitting phosphors with a broader spectra covering the red/green region, or UV-LED (380 to 420 nm) and red, green, and blue (RGB) multi-compositional phosphors are proposed.^{2,7,8} Considering these approaches, developing highly efficient phosphors with high thermal quenching temperatures and tunable color points in the entire visible region under blue or UV light excitation is urgently needed.

The alkali-earth silicate is a significant host for rare earth doped phosphors due to its inherent advantages such as excellent chemical and thermal stability as well as the low price of high-purity silicate.⁹ Moreover, silicate can be produced at

lower temperatures than nitrides and aluminates.^{10,11} M₃MgSi₂O₈ (M = Ba, Sr, Ca) compounds have attracted much attention as promising host materials for Eu²⁺-doped blue phosphors. The emission properties have been investigated for improving the intensity and chromaticity.^{12–14} The X-ray powder diffraction (XRD) data of Sr₃MgSi₂O₈ were first provided by Klasens *et al.* in 1957.¹¹ After that, G. Blasse *et al.*¹⁵ systematically investigated the photoluminescent performance of Eu²⁺ doped Me₃MgSi₂O₈ (Me = Ca, Sr, Ba) ternary system and revealed a systematic emission-color shift from blue to green depending on Me²⁺ ion size. These results are indicative of its great potential as a blue phosphor replacing commercial BaMgAl₁₁O₁₇:Eu²⁺ (BAM). In 2009, Yoshinori Yonesaki *et al.*¹⁶ firstly report the precise crystal structure of Sr₃MgSi₂O₈. It shows that Sr₃MgSi₂O₈ crystallizes in a monoclinic system, with the cell parameters $a = 13.877$ Å, $b = 5.458$ Å, $c = 9.452$ Å. Although several reports on the photoluminescence properties of Ce³⁺/Tb³⁺ or Ce³⁺/Dy³⁺ co-doped Sr₃MgSi₂O₈ phosphors have been published,^{17–19} systematic investigation on Ce³⁺ single doped Sr₃MgSi₂O₈ is still very necessary. Our study is distinguished from the previous study because of systematic investigation on the phase, crystal structure and luminescent properties of title phosphor, with some new preparation conditions and new luminescent performance accordingly.

In this paper, we report the synthesis, crystal structure and photoluminescence properties of Ce³⁺ doped Sr₃MgSi₂O₈ phosphor. The phase composition was characterized by XRD and the crystal structure is refined by structure refinement. The DRS, excitation and emission spectrum of title phosphor were measured and the mechanisms of concentration quenching and thermal quenching were discussed.

Beijing Key Laboratory of Materials Utilization of Nonmetallic Minerals and Solid Wastes, National Laboratory of Mineral Materials, School of Materials Science and Technology, China University of Geosciences, Beijing 100083, China. E-mail: liuyang@cugb.edu.cn; Fax: +86-10-82322186; Tel: +86-10-82322186



2. Experimental details

2.1 Raw materials and synthesis

The $\text{Sr}_3\text{MgSi}_2\text{O}_8:x\text{Ce}^{3+}$ phosphors were synthesized by traditional high-temperature solid-state reaction method. The starting materials are MgO (AR, Westlong Share Ltd., Guangdong, China), SrCO_3 (99.9%, Aladdin Share Ltd., Shanghai, China), SiO_2 (AR, Sinopharm Group Chemical Reagent Ltd., Shanghai, China) and CeO_2 (4 N, Minmetals Rare Earth Ltd., Beijing, China). A 5 wt% extra amount of H_3BO_3 (99.9%, Aladdin Share Ltd., Shanghai, China) was added as a flux to promote the crystallization of title phosphors. First, certain amounts of the starting materials were thoroughly grounded in an agate mortar. Then, the mixtures were placed in alumina crucibles and sintered at 1450 °C for 4 h in a flowing reducing (10 vol% H_2 /90 vol% N_2) atmosphere. Finally, the samples were furnace-cooled to room temperature and grounded into powders for further measurements.

2.2 Measurement and characterization

The phase of the title phosphor was identified by X-ray powder diffraction (XRD; D8 FOCUS diffractometer, Germany) with graphite-monochromatized Cu K α radiation ($\lambda = 1.5406 \text{ \AA}$). The photoluminescence emission (PL) and photoluminescence excitation (PLE) spectra were measured by F-4600 fluorescence spectrophotometer (Hitachi, Japan) with a photomultiplier tube functioning at 500 V and a 150 W Xe lamp as the excitation source. The spectral resolution for photoluminescence measurement was 0.2 nm. The temperature dependent luminescence properties were determined on the same spectrophotometer equipped with an automatic temperature-regulating device. Diffuse reflection spectra were obtained via a UV-3600 UV-Vis-NIR spectrophotometer (Shimadzu) connected with an integrating sphere.

3. Result and discussion

3.1 Phase and crystal structure

The phase composition of all the samples was characterized by XRD and the XRD patterns are shown in Fig. 1. The standard ICDD cards of $\text{Sr}_3\text{MgSi}_2\text{O}_8$ (PDF no. 10-0075) is also illustrated in Fig. 1 as a comparison. The diffraction peaks of the as-prepared samples were consistent with those in the standard ICDD card, suggesting that all samples were obtained as pure-phase $\text{Sr}_3\text{MgSi}_2\text{O}_8$ phase. The doping by small amounts of Ce^{3+} ions did not destroy the host crystal structure or produce foreign impurities.

To further determine the phase purity and crystal structure, the XRD patterns of $\text{Sr}_3\text{MgSi}_2\text{O}_8$ host and $\text{Sr}_3\text{MgSi}_2\text{O}_8:0.02\text{Ce}^{3+}$ phosphor were refined by the Rietveld refinement method using the Topas program. The standard structure of $\text{Sr}_3\text{MgSi}_2\text{O}_8$ is referenced as an initial structural model.¹⁶ The refinement patterns are illustrated in Fig. 2 and the main refinement parameters and detailed crystallographic data are given in Table 1. All structure refinements are convergent and end with acceptable and publishable *R* factors. The results of the

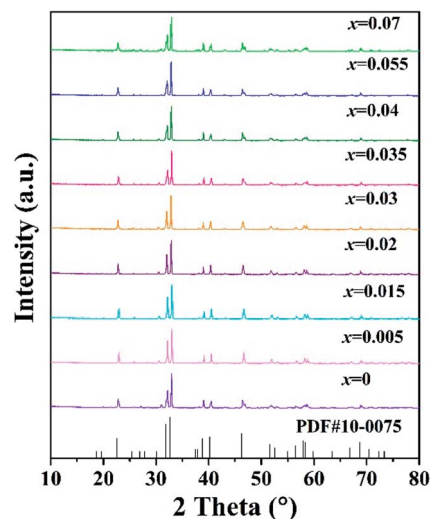


Fig. 1 XRD patterns of the as-prepared $\text{Sr}_3\text{MgSi}_2\text{O}_8:x\text{Ce}^{3+}$ ($x = 0.005, 0.015, 0.02, 0.03, 0.035, 0.04, 0.055$ and 0.07) phosphors, together with the standard ICDD cards of $\text{Sr}_3\text{MgSi}_2\text{O}_8$.

refinement further demonstrate that these phosphors match well with the starting model ($\text{Sr}_3\text{MgSi}_2\text{O}_8$) and doping of Ce^{3+} ions don't bring any impurities or foreign phases.

Based on the refinement results, the crystal structure of $\text{Sr}_3\text{MgSi}_2\text{O}_8$ host as well as the coordination environment diagram of cation in the host are presented in Fig. 3. The end-to-end $[\text{MgO}_6]$ octahedral and $[\text{SiO}_4]$ tetrahedron make up the main frame of $\text{Sr}_3\text{MgSi}_2\text{O}_8$ host, while Sr^{2+} ions are embedded between these polyhedron. Because of radius similarity between substitution Ce^{3+} and $\text{Mg}^{2+}/\text{Sr}^{2+}$, Ce^{3+} ions are considered to occupy all the Mg^{2+} and Sr^{2+} sites. To show the local crystal field environment of Ce^{3+} ions, the coordination environment diagram of Mg^{2+} and Sr^{2+} is given in Fig. 3(b–e). It's seen that Mg^{2+} ions occupy six-coordinated site while Sr^{2+} ions occupy three different sites with eight and seven-coordinated environment.

The PLE and PL spectra of the $\text{Sr}_3\text{MgSi}_2\text{O}_8:0.02\text{Ce}^{3+}$ phosphors are shown in Fig. 4. The PLE spectra of $\text{Sr}_3\text{MgSi}_2\text{O}_8:0.02\text{Ce}^{3+}$ monitored at 425 nm exhibited two distinct excitation peaks at 276 and 333 nm, which are assigned to the $4f \rightarrow 5d$ transitions of the Ce^{3+} ions. Upon excitation by near UV (n-UV) light ($\lambda_{\text{ex}} = 365 \text{ nm}$), the PL spectra exhibited an asymmetric blue emission band ranging from 380 to 550 nm with peak center at 425 nm. As shown in Fig. 4, the emission band of Ce^{3+} could be decomposed into four well-separated Gaussian components peaking at 406, 421, 442 and 468 nm, corresponding to the energy 24 649, 23 730, 22 619, 21 336 cm^{-1} , respectively. The four Gaussian components may be assigned to the emission from two different Ce^{3+} occupation sites. The energy differences between two peaks are calculated to be 2030 and 2394 cm^{-1} , respectively. The energy differences between two components are consistent with the theoretical energy difference between the separate $^2\text{F}_{5/2}$ and $^2\text{F}_{7/2}$ levels of the $4f$ ground state of Ce^{3+} due to shielding by the outer 5s and 5p



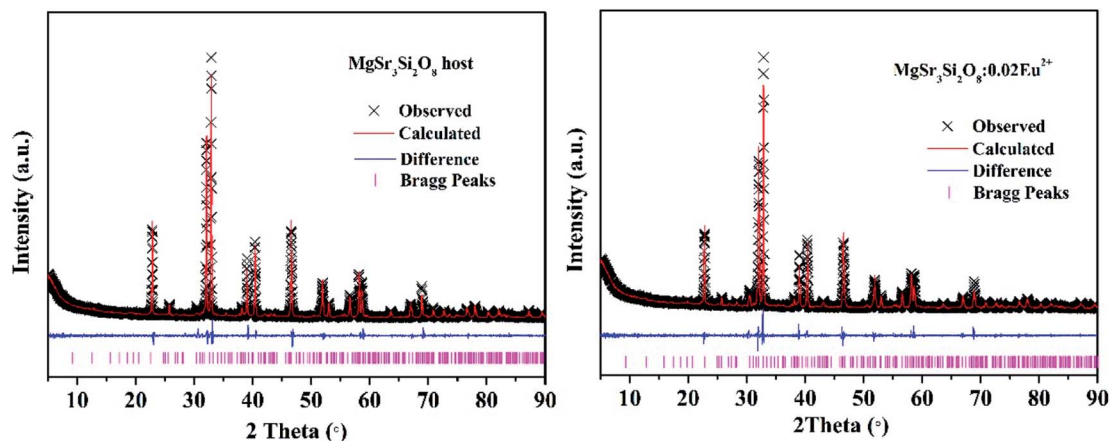


Fig. 2 XRD refinement patterns of $\text{Sr}_3\text{MgSi}_2\text{O}_8$ host (left) and $\text{Sr}_3\text{MgSi}_2\text{O}_8:0.02\text{Ce}^{3+}$ (right) phosphor. Black crosses represent the observed diffraction peak; red lines indicate the refined patterns; blue lines are residuals and purple tick marks show the Bragg positions.

Table 1 The main refinement parameters and detailed crystallographic data of $\text{Sr}_3\text{MgSi}_2\text{O}_8$ host and $\text{Sr}_3\text{MgSi}_2\text{O}_8:0.02\text{Ce}^{3+}$ phosphor

Compound	$\text{Sr}_3\text{MgSi}_2\text{O}_8$	$\text{Sr}_3\text{MgSi}_2\text{O}_8:0.02\text{Ce}^{3+}$
Crystal system	Monoclinic	Monoclinic
Space group	$P2_1/a$ (no. 14)	$P2_1/a$ (no. 14)
a (Å)	13.8724 (9)	13.8779 (69)
b (Å)	5.4565 (8)	5.4569 (27)
c (Å)	9.4516 (14)	9.4520 (49)
β (°)	90	90
2θ -interval (°)	5–90	5–90
R_{wp} (%)	8.821	8.896
R_{exp} (%)	6.871	6.761
R_{B}	2.154	1.540
GOF	1.284	1.316

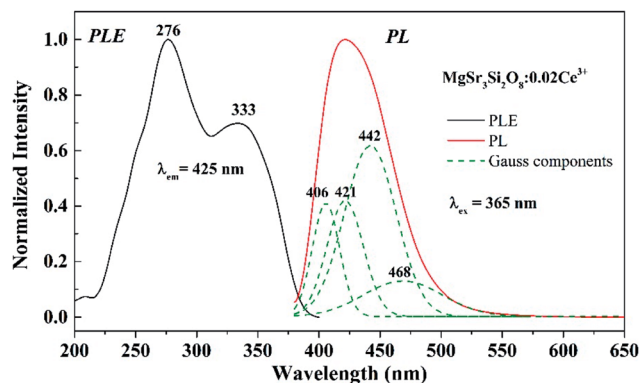


Fig. 4 PLE (left) and PL (right) spectra of the $\text{Sr}_3\text{MgSi}_2\text{O}_8:0.02\text{Ce}^{3+}$ phosphor; fitting of the emission spectra of the $\text{Sr}_3\text{MgSi}_2\text{O}_8:0.02\text{Ce}^{3+}$ phosphor is also outlined by the green dotted line.

electrons, which usually present the value as approximately 2000 cm^{-1} .⁸

The diffuse reflectance spectra (DRS) of the $\text{Sr}_3\text{MgSi}_2\text{O}_8$ host as well as the $\text{Sr}_3\text{MgSi}_2\text{O}_8:0.02\text{Ce}^{3+}$ phosphor are presented in Fig. 5. The $\text{Sr}_3\text{MgSi}_2\text{O}_8:0.02\text{Ce}^{3+}$ phosphor presents several

different absorption bands. The absorption band at approximately 220 nm is assigned to the host absorption. The several bands lying at approximately 240, 260, 310 and 350 nm are

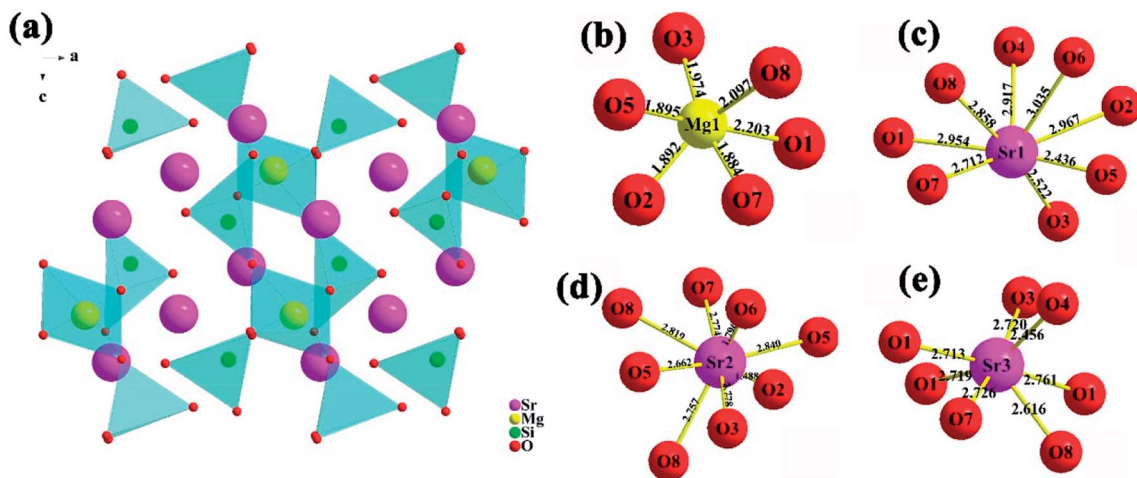


Fig. 3 (a) Schematic crystal structure of $\text{Sr}_3\text{MgSi}_2\text{O}_8$ host; (b–e) coordination environment of Mg^{2+} and Sr^{2+} sites in $\text{Sr}_3\text{MgSi}_2\text{O}_8$ host.



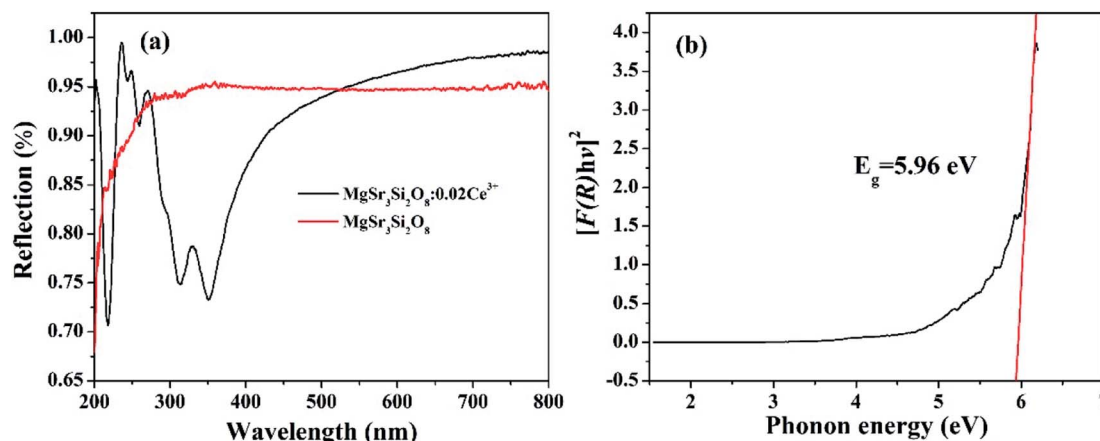


Fig. 5 (a) Diffuse reflectance spectra (DRS) of $\text{Sr}_3\text{MgSi}_2\text{O}_8$ host and $\text{Sr}_3\text{MgSi}_2\text{O}_8:0.02\text{Ce}^{3+}$ phosphor; (b) plot of transforming Kubelka–Munk function versus the energy of the light adsorbed.

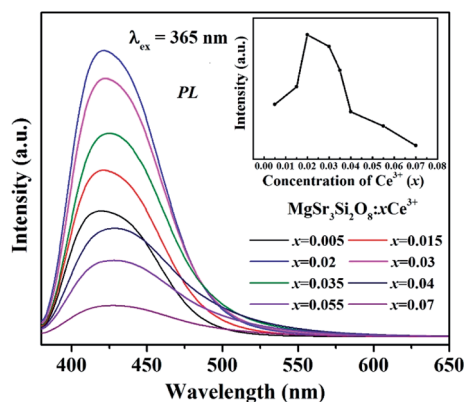


Fig. 6 PL spectra of $\text{Sr}_3\text{MgSi}_2\text{O}_8:x\text{Ce}^{3+}$ phosphors ($x = 0.005, 0.015, 0.02, 0.03, 0.035, 0.04, 0.055$ and 0.07).

attributed to the transition from the ground state to different field-splitting 5d levels of Ce^{3+} ions. The peaks at 310 and 350 nm are in agreement with two absorption peaks at 276 and 333 nm in PLE spectra. The absorption peaks corresponding 240 and 260 nm in PLE are not as obvious as those in DRS probably because the two peaks are so weak that they are covered by the strong peak at 276 nm. The band gap of $\text{Sr}_3\text{MgSi}_2\text{O}_8$ matrix was calculated according to the following equation:⁴

$$[F(R_\infty/h\nu)]^2 = C(h\nu - E_g), \quad (1)$$

where $h\nu$ indicates the energy per photon, C is a proportional constant, and E_g represents the band gap. As illustrated in Fig. 5(b), the band gap energy of the $\text{Sr}_3\text{MgSi}_2\text{O}_8$ matrix was estimated to be approximately 5.96 eV.

The PL spectra of $\text{Sr}_3\text{MgSi}_2\text{O}_8:x\text{Ce}^{3+}$ phosphors ($x = 0.005, 0.015, 0.02, 0.03, 0.035, 0.04, 0.055$ and 0.07) under 365 nm excitation are presented in Fig. 6. The emission spectra exhibit a single broad band peaks at around 425 nm based on the allowed $4f^65d \rightarrow 4f^7$ transition of Ce^{3+} ions. As shown in the

inset in Fig. 6, the emission intensity firstly rises to a maximum then falls with the increase of Ce^{3+} concentration, which is caused by the concentration quenching effect. When the doping concentration of Ce^{3+} increases, the interatomic distance between two Ce^{3+} ions becomes shorter and the energy transfer possibility is enhanced. As a result, the non-radiative transition happens between sensitizers or between sensitizer and activator, which decreases the efficiency and luminous intensity, referred to as the concentration quenching.²⁰ The optimum Ce^{3+} concentration is 2 mol%, which indicates that the $\text{Sr}_3\text{MgSi}_2\text{O}_8:x\text{Ce}^{3+}$ phosphors with optimal efficiency can be obtained at a relatively low quenching concentration.

In terms of the energy transfer between two luminous centers, the transfer mechanism may take place through three modes, including radiation reabsorption, exchange interaction and electric multipolar interaction.²¹ The mechanism of radiation reabsorption is only effective when the fluorescence and absorption spectra are broadly overlapping. Therefore, radiation reabsorption does not occur in this case. It is necessary to obtain the critical distance (R_c) for energy transfer among Ce^{3+} ions to verify the process of energy transfer in this case. According to Dexter,²² the value of the critical distance (R_c) can be reckoned via the following equation:

$$R_c \approx 2 \left(\frac{3V}{4\pi x_c N} \right)^{1/3} \quad (2)$$

here V represents the unit cell volume, x_c is critical quenching concentration and N is the number of the $\text{Mg}^{2+}/\text{Sr}^{2+}$ ions in per unit cell. Critical distance R_c is calculated as 12.62 Å by adopting the values of $V = 715.44 \text{ Å}^3$, $N = 34$ and $x_c = 0.02$. Critical distance for the exchange interaction mode is approximately 5 Å. Therefore, the exchange interaction may not play a leading role in the energy transfer within the $\text{Sr}_3\text{MgSi}_2\text{O}_8:\text{Ce}^{3+}$

Table 2 FWHMs of emission spectra of $\text{Sr}_3\text{MgSi}_2\text{O}_8:x\text{Ce}^{3+}$

x	0.005	0.015	0.02	0.03	0.035	0.04	0.055	0.07
FWHM (nm)	66.6	67.2	66.4	67.4	69.6	78.2	79.8	78.4



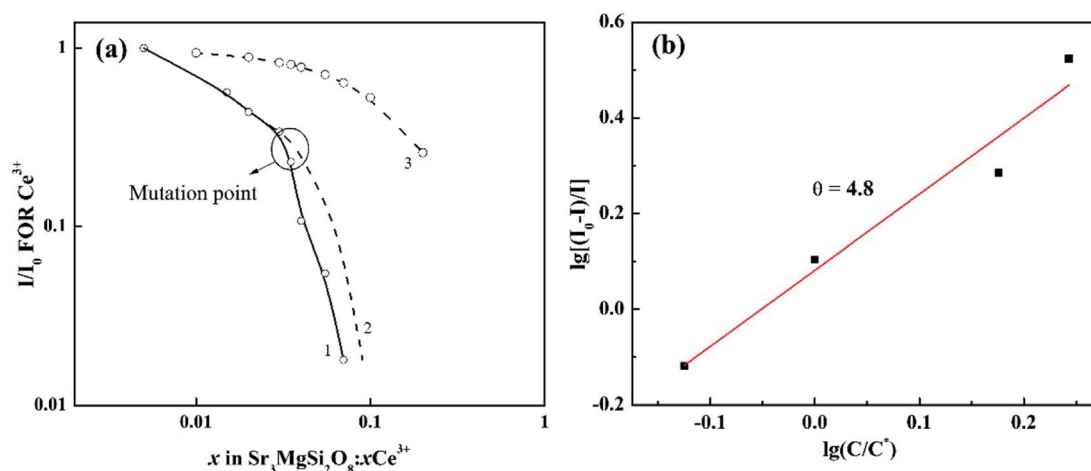


Fig. 7 (a) Normalized emission per Ce^{3+} in $\text{Sr}_3\text{MgSi}_2\text{O}_8$ host vs. Ce^{3+} concentration; curve 1 represents the actual case, curve 2 represents the expected case and curve 3 is the relation $(1-x)^6$; (b) the relationship between the $\log(C/C^*)$ and $\log[(I_0 - I)/I]$ of $\text{Sr}_3\text{MgSi}_2\text{O}_8:x\text{Ce}^{3+}$ phosphors.

phosphors. Thus, the electric multipolar interactions are dominant in the energy transfer process. According to Van Uitert,²³ the mechanism of the interaction can be explained by the following equation:

$$I/I_0 = [1 + \beta(C/C^*)^{\theta/3}]^{-1} \quad (3)$$

where I_0 represents emission per luminescent center obtained under dilute conditions; I represents emission per luminescent center at different rare earth concentration; C is the concentration of quenching ions, C^* is the critical transfer concentration of quenching ions and $\theta = 6, 8$ and 10 corresponds to dipole-dipole (d-d), dipole-quadrupole (d-q), and quadrupole-quadrupole (q-q) interactions, respectively.

From Fig. 6, we can see that emission bands widen with increasing Ce^{3+} concentration, which indicates that more sites luminescence may be involved when Ce^{3+} concentration reach a certain level. Due to different luminescence efficiency at different site, the emission intensity can be also changed. Thus, it can be erroneous to explain the mechanism of the interaction

by the eqn (3) easily. The full width at half maximum (FWHMs) of emission spectra are calculated and given in Table 2. It's clear that the FWHMs of emission spectra increase with x values, indicating that more sites luminescence may be involved with increasing Ce^{3+} concentration.

To have a better understand on the effects of more involved sites on the expression of concentration quenching by eqn (3), the normalized emission intensity I/I_0 for per Ce^{3+} vs. Ce^{3+} concentration is shown in Fig. 7(a). The exchange interaction may not play an important role in the energy transfer because curve 1 doesn't follow the relation $(1-x)^6$ (curve 3).²³ The I/I_0 usually shows a continuous smooth reducing trend with quenching ion concentration.²³ However, the curve 1 suddenly decays with an unexpected rate when x reaches 0.035. The mutation point is consistent with that in Table 2, where the FWHMs show an obvious increase after x reach 0.035. Hence, it's reasonable to conclude that when x reach a certain high level (about 0.035), Ce^{3+} ions may occupy some new sites, in which the Ce^{3+} ions may have lower luminescent efficiency. Hence, the

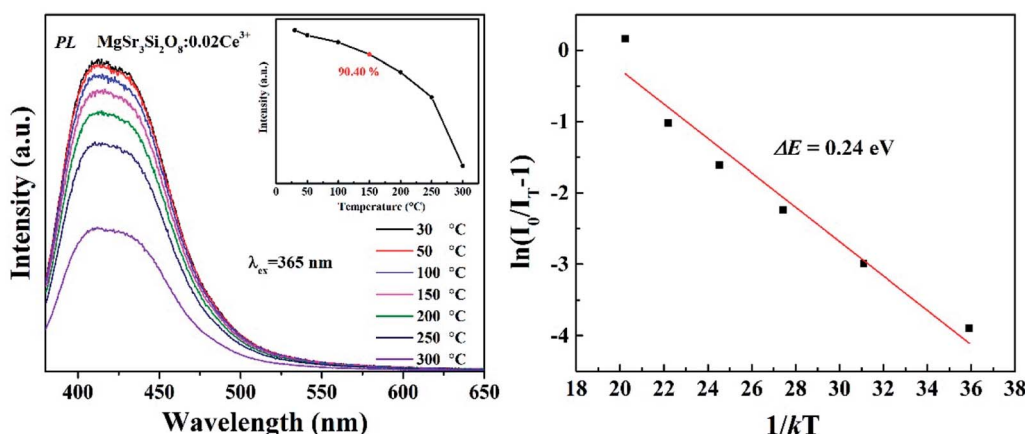


Fig. 8 (Left) Temperature-dependent PL spectra of $\text{Sr}_3\text{MgSi}_2\text{O}_8:0.02\text{Ce}^{3+}$ phosphor. The inset shows dependence of the emission intensities on temperatures; (Right) the fitting plot of $\ln(I_0/I_T - 1)$ and $1/kT$ according to Arrhenius equation.



curve 1 decays with a faster rate compared to the one it should be (as shown in curve 2). Due to the interference of this effect, only data at lower x values are adopted to calculate the multipolar interactions with eqn (3). The dependence of $\log[(I_0 - I)/I]$ on $\log(C/C^*)$ is plotted in Fig. 7(b). The value of θ is finally determined to be 4.8, indicating that the mechanism of energy transfer in $\text{Sr}_3\text{MgSi}_2\text{O}_8:x\text{Ce}^{3+}$ phosphors is mainly predominated by dipole–dipole interaction.

When functioning, the stability and reliability of a w-LED is finally determined by thermal stability of a phosphor. Good thermal stability of phosphors is always attributed to the rigid three-dimensional structure formed by polyhedron in related literatures. The temperature-dependent luminescent properties of $\text{Sr}_3\text{MgSi}_2\text{O}_8:0.02\text{Ce}^{3+}$ phosphors were measured. The activation energy, which refers to the energy barrier for non-radiative transition is an important value to estimate the thermal stability of a phosphor. Hence, the activation energy was calculated using the Arrhenius equation:

$$I_T = \frac{I_0}{1 + c \exp(-\frac{\Delta E}{kT})} \quad (5)$$

where I_0 and I_T are the emission intensity at room and measurement temperature T , respectively, c is a constant, k is the Boltzmann constant ($8.617 \times 10^{-5} \text{ eV K}^{-1}$) and ΔE is the activation energy for the thermal quenching. The temperature-dependent spectra and calculated activation energy (ΔE) are shown in Fig. 8. For $\text{Sr}_3\text{MgSi}_2\text{O}_8:0.02\text{Ce}^{3+}$, ΔE was determined to be 0.24 eV, and the luminous intensity at 150 °C was 90.4% of that at room temperature. It's obvious that the $\text{Sr}_3\text{MgSi}_2\text{O}_8:0.02\text{Ce}^{3+}$ phosphor has an excellent thermal stability.

So far, several thermal quenching processes have been proposed including thermal relaxation through the crossing point based on the configurational coordinate model, thermal ionization from the emitting $5d^1$ levels to the conduction band and direct electron transfer from (higher) $5d$ levels to the conduction band with no activation energy (photoionization of the Ce^{3+} ion) prior to relaxation to the lowest $5d^1$ state.^{8,24} Although the configuration diagram is one of the most adopted model, some papers make an argument that the photoionization in the real mechanism for thermal quenching.^{25,26}

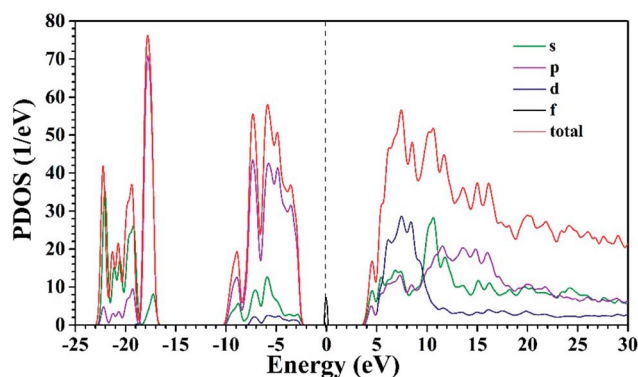


Fig. 9 Projected electronic density of states (PDOSs) of $\text{Sr}_3\text{MgSi}_2\text{O}_8:0.02\text{Ce}^{3+}$.

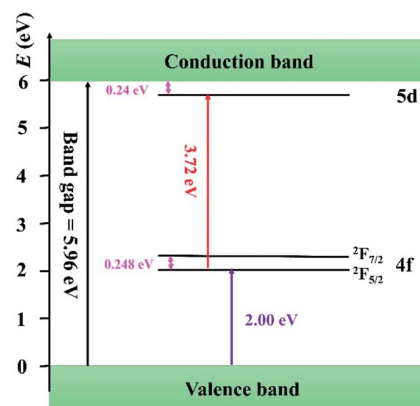


Fig. 10 Schematic energy diagram of Ce^{3+} ion in $\text{Sr}_3\text{MgSi}_2\text{O}_8$ host.

Considering this matter, the energy level position of Ce^{3+} ion in $\text{Sr}_3\text{MgSi}_2\text{O}_8$ host is calculated by first principle method. Fig. 9 illustrates the projected density of states (PDOSs) of $\text{Sr}_3\text{MgSi}_2\text{O}_8:0.02\text{Ce}^{3+}$ phosphor. The E_g is 5.72 eV. This agrees with 5.96 eV which is got from DRS. The energy gap between the $4f$ level of Ce^{3+} and the top of valence band was calculated to be 2 eV.

The diagram of the energy level position of Ce^{3+} ion in $\text{Sr}_3\text{MgSi}_2\text{O}_8$ host is given in Fig. 10. The energy gap between $4f$ of Ce^{3+} and the top of the valence band (2.00 eV) is obtained from PDOSs. The excitation energy (3.72 eV) is obtained from PLE spectra. The typically energy difference of $^2F_{5/2}$ and $^2F_{7/2}$ is around 2000 cm^{-1} (0.248 eV), which is also considered in the scheme. Considering these energy levels, it's reasonable to suppose that thermal ionization from the emitting lowest $5d$

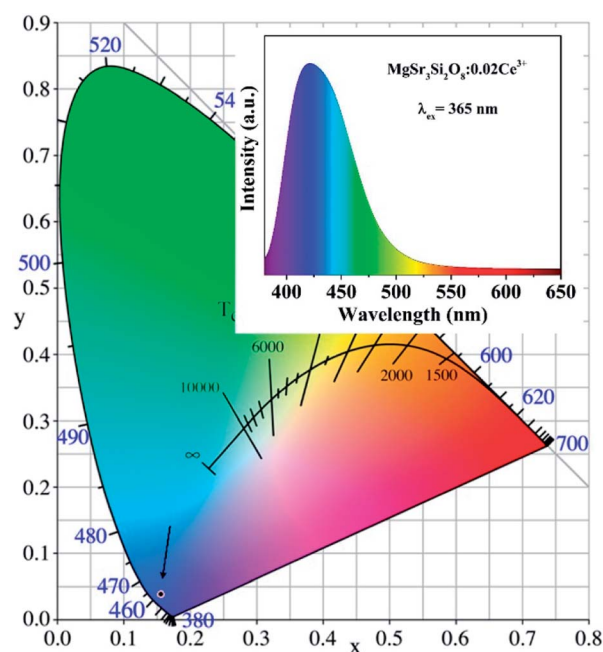


Fig. 11 CIE chromaticity diagrams of $\text{Sr}_3\text{MgSi}_2\text{O}_8:0.02\text{Ce}^{3+}$ phosphor; the inset shows the PL spectra of $\text{Sr}_3\text{MgSi}_2\text{O}_8:0.02\text{Ce}^{3+}$ phosphor with wavelength-dependent colors.



levels to the conduction band is the real mechanism of concentration quenching in the $\text{Sr}_3\text{MgSi}_2\text{O}_8$ because the small energy gap between un-relaxed lowest 5d levels and the conduction band (0.24 eV) may not result in such a high quenching temperature.

To show the real color of the as-prepared phosphors, the color rendering index (CIE) chromaticity coordinates of the $\text{Sr}_3\text{MgSi}_2\text{O}_8:0.02\text{Ce}^{3+}$ phosphor was calculated and shown in Fig. 11. It can be seen that the CIE coordinate of $\text{Sr}_3\text{MgSi}_2\text{O}_8:0.02\text{Ce}^{3+}$ phosphor lie in the blue region (0.1561, 0.0389) which demonstrates that the $\text{Sr}_3\text{MgSi}_2\text{O}_8:0.02\text{Ce}^{3+}$ can serve as a blue phosphor for w-LEDs. The PL spectra of $\text{Sr}_3\text{MgSi}_2\text{O}_8:0.02\text{Ce}^{3+}$ phosphor with wavelength-dependent colors is also presented in the inset.

To evaluate the practicability of title phosphor, the quantum efficiency (QE) of the optimal sample $\text{Sr}_3\text{MgSi}_2\text{O}_8:0.02\text{Ce}^{3+}$ is measured to be 85%, which can be made even higher by improving synthesis conditions.²⁷ As Fig. 5(a) shows, Ce^{3+} doped $\text{Sr}_3\text{MgSi}_2\text{O}_8$ phosphor has strong absorption in the UV region, which matches UV chip very well. In general, with excellent thermal stability, high QE and strong absorption in UV region, the title phosphor is deserved to be a potential blue phosphor for UV chip based w-LED.^{28,29}

4. Conclusion

The Ce^{3+} doped phosphor can be obtained by traditional high-temperature solid-state reaction method. The title phosphor crystallize in a monoclinic crystal system. The mechanism of concentration quenching was discussed and the energy transfer between Ce^{3+} ions was determined to be quadrupole–quadrupole interactions. The $\text{Sr}_3\text{MgSi}_2\text{O}_8:0.02\text{Ce}^{3+}$ title phosphor presents an excellent thermal stability. When temperature rises to 150 °C, the emission intensity can still remain 90% of that in room temperature. The thermal quenching mechanism was considered to be thermal ionization and a schematic energy levels position of Ce^{3+} ion in $\text{Sr}_3\text{MgSi}_2\text{O}_8$ host is drawn to illuminate the thermal ionization process in title phosphor.

Conflicts of interest

There are no conflicts to declare.

Acknowledgements

We thank the financial support from the National Natural Science Foundation of China (Grant No. 51472223), the National Natural Science Foundation of China (Grant No. 51772278) and the Fundamental Research Funds for the Central Universities (Grant No. 2652015020).

References

- G. Li, Y. Tian, Y. Zhao and J. Lin, Recent progress in luminescence tuning of Ce^{3+} and Eu^{2+} -activated phosphors for pc-WLEDs, *Chem. Soc. Rev.*, 2015, **44**(23), 8688–8713.

- C. C. Lin and R. S. Liu, Advances in Phosphors for Light-emitting Diodes, *J. Phys. Chem. Lett.*, 2011, **2**(11), 1268–1277.
- G. Li, C. C. Lin, W.-T. Chen, M. S. Molokeev, V. V. Atuchin, C.-Y. Chiang, *et al.*, Photoluminescence Tuning via Cation Substitution in Oxonitridosilicate Phosphors: DFT Calculations, Different Site Occupations, and Luminescence Mechanisms, *Chem. Mater.*, 2014, **26**(9), 2991–3001.
- B. Wang, Y.-g. Liu, Z. Huang and M. Fang, Energy transfer and thermal stability of Ce^{3+} , Tb^{3+} co-doped $\text{Ca}_3\text{Si}_2\text{O}_4\text{N}_2$ phosphors for white light-emitting diodes, *Chem. Phys. Lett.*, 2017, **690**, 31–37.
- B. Wang, Y. Liu, J. Chen, R. Mi, Y. Xia, Z. Huang, *et al.*, Photoluminescence properties and application of yellow $\text{Ca}_{0.65}\text{Si}_{10}\text{Al}_2\text{O}_{0.7}\text{N}_{15.3}:\text{x}\text{Eu}^{2+}$ phosphors for white LEDs, *Solid State Sci.*, 2017, **64**, 84–90.
- Z. Xia, Z. Xu, M. Chen and Q. Liu, Recent developments in the new inorganic solid-state LED phosphors, *Dalton Trans.*, 2016, **45**(28), 11214–11232.
- C.-H. Huang and T.-M. Chen, Novel yellow-emitting $\text{Sr}_8\text{MgLn}(\text{PO}_4)_7:\text{Eu}^{2+}$ ($\text{Ln} = \text{Y}, \text{La}$) phosphors for applications in white LEDs with excellent color rendering index, *Inorg. Chem.*, 2011, **50**(12), 5725–5730.
- Z. Xia and A. Meijerink, Ce^{3+} -Doped garnet phosphors: composition modification, luminescence properties and applications, *Chem. Soc. Rev.*, 2017, **46**(1), 275–299.
- X. Luo, W. Cao and F. Sun, The development of silicate matrix phosphors with broad excitation band for phosphor-converted white LED, *Sci. Bull.*, 2008, **53**(19), 2923–2930.
- Y. Liu, B. Lei and C. Shi, Luminescent properties of a white afterglow phosphor $\text{CdSiO}_3:\text{Dy}^{3+}$, *Chem. Mater.*, 2005, **17**(8), 2108–2113.
- H. A. Klasens, A. H. Hoekstra and A. P. M. Cox, Ultraviolet fluorescence of some ternary silicates activated with lead, *J. Electrochem. Soc.*, 1957, **104**(2), 93–100.
- J. S. Kim, P. Jeon, J. Choi, H. Park, S. Mho and G. Kim, Warm-white-light emitting diode utilizing a single-phase full-color $\text{Ba}_3\text{MgSi}_2\text{O}_8:\text{Eu}^{2+}$, Mn^{2+} phosphor, *Appl. Phys. Lett.*, 2004, **84**(15), 2931–2933.
- T. L. Barry, Equilibria and Eu^{2+} Luminescence of Subsolidus Phases Bounded by $\text{Ba}_3\text{MgSi}_2\text{O}_8$, $\text{Sr}_3\text{MgSi}_2\text{O}_8$, and $\text{Ca}_3\text{MgSi}_2\text{O}_8$, *J. Electrochem. Soc.*, 1968, **115**(7), 733–738.
- H.-K. Jung and K. S. Seo, Luminescent properties of Eu^{2+} -activated (Ba, Sr) $_3\text{MgSi}_2\text{O}_8$ phosphor under VUV irradiation, *Opt. Mater.*, 2006, **28**(6), 602–605.
- G. Blasse, W. L. Wanmaker, J. W. ter Vrugt and A. Bril, Fluorescence of Eu^{2+} activated silicates, *Philips Res. Rep.*, 1968, **23**, 189–200.
- Y. Yonesaki, T. Takei, N. Kumada and N. Kinomura, Crystal structure of Eu^{2+} -doped $\text{M}_3\text{MgSi}_2\text{O}_8$ ($\text{M}: \text{Ba}, \text{Sr}, \text{Ca}$) compounds and their emission properties, *J. Solid State Chem.*, 2009, **182**(3), 547–554.
- H. Yu, W. Zi, S. Lan, S. Gan, H. Zou, X. Xu, *et al.*, Green light emission by Ce^{3+} and Tb^{3+} co-doped $\text{Sr}_3\text{MgSi}_2\text{O}_8$ phosphors for potential application in ultraviolet white light-emitting diodes, *Opt. Laser Technol.*, 2012, **44**(7), 2306–2311.



- 18 H. Yu, W. Zi, S. Lan, S. Gan, H. Zou, X. Xu, *et al.*, Photoluminescence properties and energy transfer in $\text{Ce}^{3+}/\text{Dy}^{3+}$ co-doped $\text{Sr}_3\text{MgSi}_2\text{O}_8$ phosphors for potential application in ultraviolet white light-emitting diodes, *Luminescence*, 2013, **28**(5), 679–684.
- 19 Y. Chen, B. Zhou, Q. Sun, Y. Wang and B. Yan, Synthesis and luminescence properties of $\text{Sr}_3\text{MgSi}_2\text{O}_8:\text{Ce}^{3+},\text{Tb}^{3+}$ for application in near ultraviolet excitable white light-emitting-diodes, *Superlattices Microstruct.*, 2016, **100**, 158–167.
- 20 D. L. Dexter and J. H. Schulman, Theory of Concentration Quenching in Inorganic Phosphors, *J. Chem. Phys.*, 1954, **22**(6), 1063–1070.
- 21 Y.-C. Chiu, C.-H. Huang, T.-J. Lee, W.-R. Liu, Y.-T. Yeh, S.-M. Jang and R.-S. Liu, Eu^{2+} -activated silicon-oxynitride $\text{Ca}_3\text{Si}_2\text{O}_4\text{N}_2$: a green-emitting phosphor for white LEDs, *Opt. Express*, 2011, **19**(103), A331–A339.
- 22 D. L. Dexter, A Theory of Sensitized Luminescence in Solids, *J. Chem. Phys.*, 1953, **21**(5), 836–850.
- 23 I. G. V. Uitert, Characterization of Energy Transfer Interactions between Rare Earth Ions, *J. Electrochem. Soc.*, 1967, **114**, 1048–1053.
- 24 R.-J. Xie, H. T. Bert Hintzen and D. Johnson, Optical Properties of (Oxy)Nitride Materials: A Review, *J. Am. Ceram. Soc.*, 2013, **96**(3), 665–687.
- 25 P. Dorenbos, Thermal quenching of Eu^{2+} 5d–4f luminescence in inorganic compounds, *J. Phys.: Condens. Matter*, 2005, **17**(50), 8103–8111.
- 26 R. B. Jabbarov, C. Chartier, B. G. Tagiev, O. B. Tagiev, N. N. Musayeva, C. Barthou, *et al.*, Radiative properties of Eu^{2+} in BaGa_2S_4 , *J. Phys. Chem. Solids*, 2005, **66**(6), 1049–1056.
- 27 B. Wang, Y. G. Liu, Z. Huang, M. Fang and X. Wu, Discovery of novel solid solution $\text{Ca}_3\text{Si}_{3-x}\text{O}_{3+x}\text{N}_{4-2x}:\text{Eu}^{2+}$ phosphors: structural evolution and photoluminescence tuning, *Sci. Rep.*, 2017, **7**(1), 18103.
- 28 F. Kang, M. Peng, D. Y. Lei and Q. Zhang, Recoverable and Unrecoverable Bi^{3+} -Related Photoemissions Induced by Thermal Expansion and Contraction in $\text{LuVO}_4:\text{Bi}^{3+}$ and $\text{ScVO}_4:\text{Bi}^{3+}$ Compounds, *Chem. Mater.*, 2016, **28**(21), 7807–7815.
- 29 J. Han, L. Li, M. Peng, B. Huang, F. Pan, F. Kang, *et al.*, Toward Bi^{3+} Red Luminescence with No Visible Reabsorption through Manageable Energy Interaction and Crystal Defect Modulation in Single Bi^{3+} -Doped ZnWO_4 Crystal, *Chem. Mater.*, 2017, **29**(19), 8412–8424.

